

14 **Abstract.** A new weakly coupled land data assimilation (WCLDA) system based on the four-dimensional
15 ensemble variational (4D_{En}Var) method is developed and applied to the fully coupled Energy Exascale
16 Earth System Model version 2 (E3SMv2). The dimension-reduced projection four-dimensional
17 variational (DRP-4DVar) method is employed to implement 4DVar using the ensemble technique instead
18 of the adjoint technique. With an initial interest in providing initial conditions for decadal climate
19 predictions, monthly mean anomalies of soil moisture and temperature from the Global Land Data
20 Assimilation System (GLDAS) reanalysis from 1980 to 2016 are assimilated into the land component of
21 E3SMv2 within the coupled modeling framework with a one-month assimilation window. The coupled
22 assimilation experiment is evaluated using multiple metrics, including the cost function, assimilation
23 efficiency index, correlation, root mean square error (RMSE) and bias, and compared with a control
24 simulation without land data assimilation. The WCLDA system yields improved simulation of soil
25 moisture and temperature compared with the control simulation, with improvements found throughout
26 the soil layers and in many regions of the global land. In terms of both soil moisture and temperature, the
27 assimilation experiment outperforms the control simulation with reduced RMSE and higher temporal
28 correlation in many regions, especially in South America, Central Africa, Australia, and large parts of
29 Eurasia. Furthermore, significant improvements are also found in reproducing the time evolution of the
30 2012 U.S. Midwest drought, highlighting the crucial role of land surface in drought lifecycle. The
31 WCLDA system is intended to be a foundational resource for research to investigate land-derived climate
32 predictability.

33 **1 Introduction**

34 The intrinsic chaos of the atmosphere limits traditional weather forecasting to roughly two weeks
35 (Simmons and Hollingsworth, 2002). The feasibility of atmospheric predictability beyond two weeks lies
36 with the interactions of the atmosphere with slowly varying components of the Earth system such as the
37 ocean or land surface, or from predictable external forcings (Guo et al., 2012). Climate prediction can
38 therefore be conceptually divided into both an initial value and a forced boundary value problem (Collins
39 and Allen, 2002; Conil et al., 2007). One of the biggest technical challenges for improving the quality of
40 climate predictions is the initialization of coupled models from observations (Taylor et al., 2012).

41 Much work has been devoted to initializing climate system models for practicable decadal climate
42 predictions (DCPs). These models couple various components, such as models of the atmosphere, land
43 surface, ocean, sea ice, and so on. Due to their much higher complexity, coupled models are often more
44 susceptible to initial conditions (ICs) than their individual model components, underscoring the
45 importance of dedicated data assimilation (DA) (Sakaguchi et al., 2012). The capability of DA methods
46 is essential to incorporate available observations into the components of coupled model and produce the
47 optimal estimate of ICs to improve DCPs. The initialization for DCPs uses uncoupled DA and coupled
48 data assimilation (CDA) methods. Uncoupled DA performs DA under the framework of an individual
49 component model (e.g., standalone land surface model forced by atmospheric observations or reanalysis
50 data rather than coupled with an atmospheric model), and then the uncoupled DA analyses from different
51 individual components are combined to form the ICs of a coupled model (Zhang et al., 2020). For
52 example, most existing reanalysis data were produced using uncoupled DA approaches, and these
53 reanalysis datasets are then directly used to initialize DCPs in some studies (Du et al., 2012; Bellucci et
54 al., 2013). However, such uncoupled DA often exhibits poor consistency among the ICs of different
55 component models, and eventually produces low prediction skills (Balmaseda et al., 2009; Boer et al.,
56 2016; Ardilouze et al., 2017).

57 To obtain balanced multi-component ICs in coupled models, recent studies focus on the
58 development of CDA methods under the coupled modeling framework (Penny and Hamill, 2017; He et
59 al., 2020a). The purpose of CDA is to produce balanced and coherent ICs for all components within the
60 climate system by incorporating observational information from one or more components in the coupled

61 model, providing great potential for improving seamless climate predictions (Dee et al., 2014). Some
62 studies underscore the superior advantages of CDA over traditional uncoupled DA methods (Lea et al.,
63 2015; Zhang et al., 2005). CDA methods are categorized into two main types: weakly coupled data
64 assimilation (WCDA) and strongly coupled data assimilation (SCDA). WCDA assimilates the
65 observations or existing reanalysis into the respective component of the coupled model and then transfers
66 the observational information to the other components through the coupled model integration (He et al.,
67 2020b; Zhang et al., 2020). Considering that sequential DA encompasses both the analysis and the
68 forecast steps, WCDA allows no direct influence of observations from a single component to other
69 components in the analysis step as the cross-component background error covariances are not used, but
70 coupling in the forecast step allows interactions across different components during the model integration
71 (Browne et al., 2019) and propagates the observational information to other components. In contrast,
72 SCDA utilizes cross-component background error covariances to directly assimilate the observational
73 information from one component into all components, treating the entire Earth system model as one
74 unified system (Penny et al., 2019). Furthermore, similar to WCDA, SCDA also allows coupling in the
75 forecast step to propagate the observations from one component to the other components (Yoshida and
76 Kalnay, 2018). Several studies indicate that SCDA typically exhibits more pronounced improvements in
77 assimilation performance relative to WCDA (Smith et al., 2015; Sluka et al., 2016). However, the
78 application of SCDA poses substantial technical challenges, particularly in the establishment of effective
79 cross-component background error covariances. Consequently, the majority of contemporary CDA
80 systems still utilize the WCDA framework.

81 Recent research efforts have started to implement the CDA system to initialize DCPs, using a
82 diverse range of DA techniques from simple to complex. The simplest method is nudging which adjusts
83 the model states towards the observations or existing reanalysis (Hoke and Anthes, 1976; Zhang et al.,
84 2020). Although the nudging method is time-saving and easy to implement, its application in CDA is
85 restricted primarily due to the limited types of observations and the required interpolation of observations
86 at every time step of model integration (He et al., 2017). Previous studies have developed advanced CDA
87 systems using variational and filtering approaches, such as the three-dimensional variational data
88 assimilation (3DVar) (Laloyaux et al., 2016; Yao et al., 2021), and ensemble-based techniques like the

89 ensemble Kalman filter (EnKF) (Zhang et al., 2007). The former generally utilizes the stationary
90 background error covariance and assimilates observations sequentially (Lin et al., 2017). In contrast, the
91 latter uses the flow-dependent forecast error covariance and recursively integrates observations into the
92 model (Lei and Hacker, 2015). Several studies also show encouraging progress in constructing CDA
93 systems using four-dimensional variational data assimilation (4DVar) method (Smith et al., 2015; Fowler
94 and Lawless, 2016). The objective of 4DVar is to optimize four-dimensional model states and provide a
95 compatible temporal trajectory that matches observational records across each assimilation window
96 (Mochizuki et al., 2016). The 4DVar method is an advanced assimilation technique that exhibits
97 superiority over other assimilation techniques like nudging and 3DVar in multiple aspects. Initial shocks
98 that influence prediction skills can be significantly minimized by the 4DVar approach due to the
99 dynamical consistency between the model and ICs (Sugiura et al., 2008). However, it is difficult to apply
100 the 4DVar method for CDA systems in the fully coupled model because of the challenge in adjoint
101 integration of the coupled model and its high computational cost in the analysis step. Finally, to capitalize
102 on the strengths of both ensemble and variational techniques, recent studies focus on developing new
103 hybrid data assimilation methods (Wang et al., 2010; Buehner et al., 2018). The hybrid approach utilizes
104 an ensemble forecast to generate flow-dependent forecast error covariances and presents a way to
105 perform 4DVar optimization without the need for tangent linear and adjoint models (Lorenc et al., 2015).
106 However, most studies on CDA have focused on assimilating observations or reanalysis data of ocean,
107 atmosphere and even sea ice. There have been relatively few instances of CDA studies assimilating land
108 observations or reanalysis data.

109 In this study, we introduce the development of the 4DEnVar-based weakly coupled land data
110 assimilation (WCLDA) system for the Energy Exascale Earth System Model version 2 (E3SMv2) (Golaz
111 et al., 2022). The 4DEnVar method in this WCLDA system is the dimension-reduced projection 4DVar
112 (DRP-4DVar; Wang et al., 2010) which utilizes the ensemble technique as an alternative to the adjoint
113 technique for implementing 4DVar. In this WCLDA system, monthly mean anomalies of soil moisture
114 and temperature from a global land reanalysis product are assimilated into the land component of a
115 coupled climate model in the analysis step, and subsequently during the forecast step, the land reanalysis
116 information incorporated into the ICs of the land component is propagated to the other components (e.g.,

117 atmosphere and ocean) through the fully coupled model integration and influences the ICs of all
118 components for the next assimilation window. The primary goal of the WCLDA system is intended to be
119 a foundational resource for exploring predictability of the Earth system by the E3SM community,
120 specifically focusing on understanding the sources of predictability provided by land versus ocean, with
121 an initial focus on DCPs. This WCLDA system also provides the groundwork for future actionable
122 predictions of Earth system variability using E3SM.

123 The objective of this paper is to introduce the implementation of the 4DEnVar-based WCLDA
124 system for the land component of E3SMv2. In Section 2, we provide an overview of the E3SMv2 model,
125 describe the 4DEnVar methodology in detail and outline the framework of the 4DEnVar-based WCLDA
126 system. Preliminary evaluation of the WCLDA system is presented in Section 3. Finally, major
127 conclusions are discussed in Section 4.

128

129 **2 Methods**

130 **2.1 Model Description**

131 The model used in this study is a relatively new state-of-the-art Earth system model known as
132 Energy Exascale Earth System Model version 2 (E3SMv2), supported by the U.S. Department of Energy
133 (DOE) to improve actionable Earth system predictions and projections (Leung et al., 2020). The
134 atmospheric component is the E3SM Atmosphere Model version 2 (EAMv2), which is built on the
135 spectral-element atmospheric dynamical core with 72 vertical levels (Dennis et al., 2012; Taylor et al.,
136 2020). At the standard resolution, EAMv2 is applied on a cubed sphere with a grid spacing of ~100 km
137 for the dynamics. The ocean component is the Model for Prediction Across Scales-Ocean (MPAS-O),
138 which applies the underlying spatial discretization to the primitive equations with 60 layers using a z-
139 star vertical coordinate (Petersen et al., 2018; Reckinger et al., 2015). The sea ice component is MPAS-
140 SI, which shares the same Voronoi mesh with MPAS-O, with mesh spacing varying between 60km in the
141 mid-latitudes and 30 km at the equator and poles (Golaz et al., 2022). The land component is the E3SM
142 Land Model version 2 (ELMv2), which is based on the Community Land Model version 4.5 (CLM4.5)
143 (Oleson et al. 2013). Simulations are run in a satellite phenology mode with prescribed leaf area index,
144 and the prescribed vegetation distribution has been updated for better consistency between land use and

145 changes in plant functional types described by Golaz et al. (2022). The river transport component is the
146 Model for Scale Adaptive River Transport version 2 (MOSARTv2), which provides detailed
147 representation of riverine hydrologic variables (Li et al., 2013). These five components exchange fluxes
148 through the top-level coupling driver version 7 (CPL7) (Craig et al., 2012). Further details on the
149 E3SMv2 model are described in Golaz et al. (2022).

150

151 **2.2 Land Reanalysis Dataset**

152 Monthly mean soil moisture and soil temperature data in a total of ten soil layers are produced by
153 the Global Land Data Assimilation System (GLDAS; Rodell et al., 2004). The GLDAS product generates
154 optimal fields of land surface states and fluxes in near-real time by forcing multiple offline land surface
155 models with observation-based data fields. These reliable and high-resolution global land surface datasets
156 from GLDAS are extensively utilized in weather and climate studies, hydrometeorological investigations
157 and water cycle research (Chen et al., 2021; Zhang et al., 2018). The GLDAS datasets have been available
158 globally at high spatial resolution since January 1979 and can be accessed through the Goddard Earth
159 Science Data and Information Service Center. For more consistency with ELM, we utilize GLDAS data
160 produced by CLM.

161 Current initialization techniques are broadly classified into two categories: full-field assimilation
162 with observed values, and anomaly assimilation with observed anomalies (Hu et al., 2020; Polkova et al.,
163 2019). The full-field assimilation is commonly performed to reduce the influence of systematic model
164 biases by replacing the initial model state with the optimal available estimate of the observed state (Volpi
165 et al., 2017). However, the model trajectory tends to drift away from the observations and revert to the
166 model's inherent preferred state because of model deficiencies (Smith et al., 2013). This problem is
167 partially addressed with the anomaly assimilation by assimilating the observed anomalies added to the
168 model climatology (Carrassi et al., 2014). In this study, we conduct the anomaly assimilation for the
169 WCLDA system with bias correction applied to GLDAS data before assimilation. For bias correction,
170 the difference between GLDAS data and its long-term average is calculated as anomalies and then added
171 to the simulated model climatology.

172

173 **2.3 Data Assimilation Scheme**

174 The 4DEnVar algorithm in this study is based on the DRP-4DVar technique, which is an efficient
 175 pathway for applying 4DVar through using the ensemble method rather than the adjoint technique (Wang
 176 et al., 2010). The DRP-4DVar method generates the optimal estimation in the sample space through
 177 aligning the observations with ensemble samples along the coupled model trajectory (Liu et al., 2011).

178 DRP-4DVar is an economical approach that minimizes the cost function of the standard 4DVar by
 179 using the ensemble technique instead of the adjoint technique (Wang et al., 2010). The background error
 180 covariance matrix B is estimated using the pure ensemble covariance. The ensemble members originate
 181 from historical or ensemble forecasts. Considering the high computational cost of ensemble forecasts for
 182 the coupled model in our study, we utilize outputs from the pre-industrial control (PI-CTRL) experiment
 183 of E3SMv2 to generate ensemble members. The instantaneous state at the beginning of each month and
 184 the corresponding monthly mean state of this month from the 100-year balanced PI-CTRL simulation
 185 are used as the samples of initial condition (x_i) and forecast samples (y_i). The corresponding perturbation
 186 samples are calculated as $x'_i = x_i - \bar{x}$ and $y'_i = y_i - \bar{y}$, where \bar{x} and \bar{y} are the 100-year average
 187 values of x_i and y_i at the same month, respectively. Then, m pairs of perturbation samples
 188 ($x'_1, x'_2, x'_3, \dots, x'_m$) and ($y'_1, y'_2, y'_3, \dots, y'_m$) are selected at each DA analysis step according to the
 189 correlations between y'_i and the observational innovation $y'_{obs} = y_{obs} - y_b$ and the independence
 190 between y' samples. In this study, $m = 30$. Then the estimation of the background error covariance
 191 matrix B is represented by the formula in Eq. (1), utilizing the selected x' samples. To remove the
 192 spurious remote correlations in the B matrix, the localization approach is applied to optimize the
 193 assimilation performance (Wang et al., 2018).

$$194 \quad \begin{cases} B = bb^T \\ b = \frac{1}{\sqrt{m-1}} \times (x'_1 - \bar{x}', x'_2 - \bar{x}', x'_3 - \bar{x}', \dots, x'_m - \bar{x}') \\ \bar{x}' = \frac{1}{m} (x'_1 + x'_2 + x'_3 + \dots + x'_m) \end{cases} \quad (1)$$

195 According to Wang et al. (2010), DRP-4DVar produces the analysis increment (x'_a) by minimizing
 196 the 4DVar cost function in the incremental form (Courtier et al., 1994):

$$197 \quad \begin{cases} J(x'_a) = \min_{x'} J(x') \\ J(x') = \frac{1}{2} (x')^T B^{-1} x' + \frac{1}{2} (\tilde{y}' - \tilde{y}'_{obs})^T (\tilde{y}' - \tilde{y}'_{obs}) \end{cases} \quad (2)$$

198 Here $x' = x - x_b$ represents the increment of model variables relative to the background; $\tilde{y}'_{obs} =$

199 $r^{-1}y'_{obs} = r^{-1}(y_{obs} - y_b)$ denotes the weighted observational innovation for monthly mean anomalies
 200 of soil moisture and temperature, and $R = rr^T$ is the observational error covariance matrix that is
 201 usually diagonal; $\tilde{y}' = r^{-1}y' = r^{-1}(y - y_b)$ is the weighted projection of the increment (x') onto the
 202 observation space; the superscript T represents the transpose.

203 To simplify the calculation of the minimization, the increment of model state variables x' and the
 204 corresponding weighted observation increment \tilde{y}' are projected onto the dimension-reduced sample
 205 space through the following projection transformations:

$$206 \quad \begin{cases} x' = P_x \alpha \\ \tilde{y}' = P_y \alpha \end{cases} \quad (3)$$

207 where α is the m -dimension column vector containing the weight coefficients $(\alpha_1, \alpha_2, \alpha_3, \dots, \alpha_m)$; P_x
 208 and P_y denote the projection matrices that incorporate the initial condition perturbations and the
 209 corresponding monthly mean samples as follows:

$$210 \quad \begin{cases} P_x = (x'_1, x'_2, x'_3, \dots, x'_m) \\ P_y = (\tilde{y}'_1, \tilde{y}'_2, \tilde{y}'_3, \dots, \tilde{y}'_m) \end{cases} \quad (4)$$

211 where $\tilde{y}'_i = r^{-1}y'_i$ ($i = 1, 2, \dots, m$). Then the original 4DVar cost function defined in Eq. (2) is
 212 transformed into the following new cost function and the analysis can be computed in the sample space
 213 by minimizing this new cost function:

$$214 \quad \begin{cases} \tilde{J}(\alpha_a) = \min_{\alpha} \tilde{J}(\alpha) \\ \tilde{J}(\alpha) = \frac{1}{2} \alpha^T B_{\alpha}^{-1} \alpha + \frac{1}{2} (P_y \alpha - \tilde{y}'_{obs})^T (P_y \alpha - \tilde{y}'_{obs}) \\ x_a = x_b + x'_a = x_b + P_x \alpha_a \end{cases} \quad (5)$$

215 The solution to this minimization problem is formulated as:

$$216 \quad \alpha_a = (B_{\alpha}^{-1} + P_y^T P_y)^{-1} P_y^T \tilde{y}'_{obs} \quad (6)$$

217 In this study, the DRP-4DVar-based WCLDA system is used to incorporate the land reanalysis data only.

218 The optimal analysis for the land state variables (x_a^{lnd}) is obtained by adding the analysis increment
 219 (x'_a^{lnd}) to the background of land ICs (x_b^{lnd}), as expressed in Eq. (7):

$$220 \quad x_a^{lnd} = x_b^{lnd} + x'_a^{lnd} = x_b^{lnd} + P_x (B_{\alpha}^{-1} + P_y^T P_y)^{-1} P_y^T \tilde{y}'_{obs} \quad (7)$$

221 In the analysis step, only the land state variables are updated to the optimal analysis (x_a^{lnd}).

222 Subsequently, we proceed with a one-month freely coupled integration of the E3SMv2 model during the

223 forecast step. This integration is initialized from the optimal land ICs (x_a^{lnd}) along with the background

224 fields as the ICs of other components (e.g., atmosphere and ocean). Throughout this one-month free

225 integration, the interactions among the model components indirectly enhance the background states of
226 these components (e.g., atmosphere and ocean) for the next assimilation window due to the more realistic
227 land state variables. Moreover, this coupled integration also contributes to the balance between the ICs
228 of different components.

229

230 **2.4 4DVar-based WCLDA System**

231 The 4DVar-based WCLDA system is developed to assimilate the monthly mean soil moisture and
232 temperature data from the GLDAS analysis dataset into the land component of E3SMv2 using the DRP-
233 4DVar method. Two sets of numerical experiments are conducted to evaluate the performance of land
234 data assimilation in the WCLDA system. The control simulation (CTRL) is a 37-year freely coupled
235 integration driven by observed external forcings (e.g., solar radiation, greenhouse gas and aerosol
236 concentrations) from 1980 to 2016. In the freely coupled simulation, the various components of the Earth
237 system model, namely the atmosphere, land, river, ocean, and sea ice, interact dynamically without any
238 restraints. The observed external forcing mainly acts on the atmospheric component and then influences
239 other components (e.g., land surface, ocean, and sea ice) through their coupling with the atmosphere.
240 CTRL provides the benchmark for assessing the performance of the WCLDA system. The assimilation
241 experiment (Assim) is conducted from 1980 to 2016 based on the WCLDA system in which the GLDAS
242 data are assimilated into the land state variables from the first to the tenth layer with a one-month
243 assimilation window under the coupled modeling framework. The effectiveness of the WCLDA system
244 is evaluated through the comparison between Assim and CTRL. In both Assim and CTRL, the transient-
245 historical external forcings are prescribed following the CMIP6 protocol (Eyring et al., 2016). In contrast
246 to decadal timescales, data signals with temporal resolutions shorter than one month can potentially
247 introduce undesirable noise, which can adversely affect DCPs when high temporal resolution data are
248 assimilated into the ICs. Moreover, it is very computationally demanding to assimilate complex actual
249 observations in the initialization for DCPs that requires long-term DA cycles. Therefore, similar to most
250 existing initialization approaches for DCPs that assimilate reanalysis data, this study describes the
251 implementation of a data assimilation approach for initializing DCPs by assimilating monthly mean
252 GLDAS data within the one-month assimilation window.

253 The flowchart of the 4DEnVar-based WCLDA system is illustrated in Figure 1. The DRP-4DVar
254 method incorporates three inputs: model background, observational innovation and 30 perturbation
255 samples. First, the E3SMv2 model is executed for one month, during which state variables such as model
256 background (x_b), observational operator (H) and observational background (y_b) are stored. The model
257 background (x_b) denotes the monthly initial states before assimilation, and the observational operator (H)
258 represents a one-month integration by the coupled model to generate monthly mean model outputs (y_b).
259 Second, upon completion of the one-month coupled run, the observational innovation (\tilde{y}'_{obs}) is determined
260 by calculating the differences in soil moisture and temperature between the monthly mean GLDAS data
261 (y_{obs}) and the model outputs (y_b). From the 100-year sample database of the E3SMv2 PI-CTRL
262 simulation, 30 samples of monthly mean perturbation (\tilde{y}') are chosen with the highest absolute correlation
263 with the observational innovation. The corresponding 30 monthly IC samples (x') are also obtained.
264 Finally, the analysis increment is generated in the sample space and the optimal analysis (x_a) is calculated
265 using the DRP-4DVar algorithm. To alleviate spurious correlations, a localization scheme is implemented
266 in the DRP-4DVar-based WCLDA system (Wang et al., 2018).

267 The schematic diagram in Figure 2 outlines the assimilation process of the 4DEnVar-based WCLDA
268 system in E3SMv2. The incorporation of GLDAS data into the E3SMv2 model consists of the analysis
269 step and the forecast step. In the analysis step, the differences between monthly mean GLDAS data and
270 model outputs are calculated and utilized to produce the optimal assimilation analysis at the beginning of
271 a one-month assimilation window. Subsequently, in the forecast step, this optimal assimilation analysis is
272 used as the land ICs combined with the background ICs for other components to conduct one-month
273 forecast using the E3SMv2 model. This forecast generates the backgrounds of all model components for
274 the next assimilation window. As a result, the forecasted backgrounds for all components are influenced
275 by the land reanalysis information incorporated into the ICs of the land component. In general, when the
276 coupled model is used in the forecast step while the optimal assimilation analysis is updated separately
277 for the respective component, the assimilation approach is identified as WCDA (Penny et al., 2019; Zhang
278 et al., 2020).

279 The detailed assimilation process mainly consists of three steps within each one-month assimilation
280 window: 1) the E3SMv2 model is initially executed for one month to generate the simulated monthly

281 mean soil moisture and temperature (y_b^{lnd}); 2) the observational innovation (y'_{obs}) is obtained through
 282 subtracting the model simulation (y_b^{lnd}) from the monthly mean observation (y_{obs}^{lnd}). This innovation is
 283 then applied to formulate the optimal assimilation analysis of land surface (x_a^{lnd}) at the beginning of the
 284 assimilation window through the DRP-4DVar method; 3) the E3SMv2 model is rewound to the start of
 285 the month and the second one-month model run is executed using the optimal ICs (x_a) to generate the
 286 background for the next assimilation window. Due to multi-component interactions during the one-month
 287 freely coupled integration, the land reanalysis information can potentially benefit other components (e.g.,
 288 atmosphere and ocean) in the coupled modeling framework (Li et al., 2021; Shi et al., 2022). To assimilate
 289 the monthly mean GLDAS product, fully coupled integration by the E3SMv2 model is performed twice
 290 within each one-month assimilation window: first to generate the observational innovation by computing
 291 the differences between the GLDAS data and model outputs for analysis, and second to forecast the
 292 backgrounds of all components for the next assimilation window. When the fully coupled model is
 293 executed for the second one-month run, the land reanalysis information is transferred to the other
 294 components through multi-component interactions. This approach is similar to previous studies that
 295 employed the "two-step" scheme in which the land model integration is performed twice within the same
 296 month to assimilate the monthly GRACE-based TWS observations (Houborg et al., 2012; Giroto et al.,
 297 2016).

298

299 **2.5 Evaluation Metrics**

300 The reduction rate of the cost function is a significant metric for verifying the effectiveness of the
 301 WCLDA system and evaluating the extent of observational information assimilated by the coupled model,
 302 which is formulated as:

$$303 \quad \begin{cases} \frac{J_1 - J_0}{J_0} \times 100\% \\ J_0 = \frac{1}{2} (y_{obs} - y_b)^T R^{-1} (y_{obs} - y_b) \\ J_1 = \frac{1}{2} (y_{obs} - y_a)^T R^{-1} (y_{obs} - y_a) \end{cases} \quad (8)$$

304 where J_0 and J_1 denote the observational cost function before and after assimilation respectively, y_{obs}
 305 represents the GLDAS data, y_a denotes the monthly mean analyses, y_b is the observation-space
 306 background, and R is defined as the observation error covariance matrix. Negative value for this metric
 307 indicates that observational information has been correctly incorporated into the model variables.

308 Following Yin et al. (2014), the assimilation efficiency (AE) index is defined to evaluate the efficiency
309 of the WCLDA system as follows:

$$310 \quad AE = \frac{RMSE_{Assim}}{RMSE_{CTRL}} - 1 \quad (9)$$

311 In this equation, $RMSE_{Assim}$ is the root mean square error (RMSE) between Assim and the reference data,
312 while $RMSE_{CTRL}$ represents the RMSE between CTRL and the reference data. Negative (positive) AE
313 value indicates improvements (degradations) by the assimilation. In the following sections, we use the
314 GLDAS data as the main reference data to verify the correctness of the WCLDA system, but some
315 analyses are also performed using MODIS surface soil moisture and land surface temperature as the
316 reference data.

317

318 **3 Results**

319 **3.1 Evaluation of the cost function**

320 Figure 3 displays the time series of the monthly reduction rate of the cost function in the 4DEnVar-
321 based WCLDA system. In the first month, the reduction rate reaches approximately 26.06% in Assim.
322 Over the subsequent months, Assim maintains the average reduction rate of 7.73% throughout the entire
323 37-year period. Furthermore, negative reduction rates are observed in 98.65% of the total months,
324 indicating the effectiveness of the WCLDA system. These results suggest that the WCLDA system is
325 correctly implemented, with the observational data successfully assimilated into the coupled model.

326

327 **3.2 Evaluation of the AE index**

328 The spatial pattern of the AE index for soil moisture at different depths is depicted in Figure 4. The
329 AE value exhibits negative signal in most areas for total ten soil layers, suggesting the reduction in RMSE
330 for soil moisture after assimilation. Significant improvements appear over North America, South America,
331 southern Africa, Europe, and Asia. However, assimilation performance is degraded in the northern part of
332 Russia and northern Africa. This is consistent with the findings in other studies that assimilation updates
333 in northern Russia are limited due to the complexities of accurately representing frozen ground and snow
334 processes in high latitudes (Edwards et al., 2007; Ireson et al., 2013). As surface soil moisture is highly
335 susceptible to atmospheric conditions, assimilation performance of surface soil moisture is limited by the

336 accuracy of atmospheric forcing. Furthermore, some degradations found in the deep layers could be
337 attributed to the substantial influence of various terrestrial factors, such as subsurface runoff and
338 interactions with groundwater, similar to the findings in previous studies (Liu and Mishra, 2017; Zeng
339 and Decker, 2009).

340 Figure 5 shows the spatial distribution of the AE index for soil temperature from surface to deep
341 layers. Most grid cells from the ten soil layers are dominated by negative AE signals, indicating improved
342 performance for soil temperature after assimilation. Moreover, the spatial patterns across different soil
343 layers are highly consistent with each other and exhibit similar magnitudes in most areas. Notable
344 improvements are observed in central Europe, South America, eastern Russia, and large parts of Eurasia
345 and North America. In contrast, slight degradations appear over Southeast Asia and along the northern
346 fringes of Africa. This may be partly related to model uncertainties and possible atmospheric noise, as
347 shown by many past studies (Kwon et al., 2016; Lin et al., 2020).

348 We further perform an analysis of the spatial pattern of the AE index for surface soil moisture and
349 land surface temperature between MODIS data and model simulations (Figure A1). For surface soil
350 moisture, the comparison with MODIS data suggests that the majority of global regions exhibit reduced
351 RMSE after assimilation. The reduction of RMSE is pronounced in central North America, South America,
352 southern Africa, Australia, and Europe. However, in high-latitude areas, significant degradations are
353 observed in northern Russia, which may be possibly related to model deficiencies in simulating the
354 complex frozen ground and snow processes (Edwards et al., 2007; Ireson et al., 2013). Regarding land
355 surface temperature, improved performances are evident over South America, Australia, southern Africa,
356 and large parts of Eurasia when compared to MODIS data. In contrast, some degradations appear over
357 parts of North America and central Asia, which still require further improvement.

358

359 **3.3 Evaluation of the correlation**

360 Figure 6 displays the spatial patterns of the differences in temporal correlations for soil moisture
361 between Assim and CTRL with observations across different soil layers. The majority of global regions
362 in Assim exhibit higher correlations from the first to the tenth layer compared with CTRL, suggesting the
363 overall good performance of the WCLDA system. Enhanced correlations in deep soil layers are more

364 pronounced than in shallow layers, which may be attributed to the longer memory of soil processes in the
365 deeper soil layers (Wang et al., 2010). Improved correlations appear over North America, central Europe,
366 Asia, and parts of Africa. However, some scattered areas show slight degradations, such as northern South
367 America, central Africa, and eastern Russia. Overall, Assim outperforms CTRL with higher correlation
368 (Figure 6) and lower RMSE (Figure 4) in many regions, such as Europe, North America, southern South
369 America, and South Asia.

370 The correlation differences in soil temperature between Assim and CTRL from surface to deep
371 layers are shown in Figure 7. Assim yields improved correlations from the first to the tenth layer across
372 the majority of global regions. Furthermore, similar spatial patterns and magnitudes are observed in the
373 performance of different soil layers, implying the significant heat transfer from the surface to deep zone
374 that constrains soil temperature across the soil column. Notable improvements are located over South
375 America, central Africa, Australia, central Europe, and East Asia. Nevertheless, some degradations
376 appear over North America, western Europe, and Northeast China. Assim shows superior performance
377 over CTRL for soil temperature with higher correlation (Figure 7) and lower RMSE (Figure 5) in many
378 regions, including South America, central Europe, Australia, and central Africa.

379

380 **3.4 RMSE and bias of the global mean soil moisture and temperature**

381 The vertical distributions of RMSE differences between Assim and CTRL for soil moisture and
382 temperature are evaluated in Figure 8. Compared with CTRL, Assim shows noticeable improvements
383 with reduced RMSE for both soil moisture and temperature in all ten soil layers. For soil moisture, the
384 reduction of RMSE increases with depth from the upper to deep soil layers, reaching its maximum at the
385 tenth layer. This could be attributed to the longer soil memory in deep layers than shallow layers. For soil
386 temperature, the reduction of RMSE exhibits similar magnitude from the surface to deep soil layers, which
387 may be explained by the significant heat transfer across different soil layers in regulating soil temperature
388 throughout the soil column.

389 Figure 9 shows the time evolutions of the vertically averaged global mean soil moisture and
390 temperature bias and RMSE differences. For soil moisture bias (Figure 9a), CTRL exhibits dry biases
391 during the first twenty years and wet biases afterwards. In contrast, Assim shows smaller biases during

392 both periods by reducing the dry bias prior to ~2000 and the wet bias thereafter. Assim also exhibits
393 reduced RMSE (Figure 9b) for soil moisture throughout the entire 37-year period. For soil temperature
394 bias (Figure 9c), CTRL and Assim display comparable performances, possibly due to the small magnitude
395 of model deviation in soil temperature. The RMSE differences (Figure 9d) suggest that Assim decreases
396 the RMSE for soil temperature in the majority of months, with 74.10% of the total months in Assim
397 exhibiting lower RMSE than CTRL. In summary, the superior performance for both soil moisture and
398 temperature in Assim demonstrates that land reanalysis information has been effectively incorporated into
399 the model variables through the WCLDA system.

400 Noticeably, the simulated soil temperature and soil moisture display similar long-term trends, with
401 cold and dry biases before ~2000 and warm and wet biases afterwards. The soil temperature biases may
402 be related to the global surface air temperature simulated in E3SMv2, which is notably too cold compared
403 to the observed record during the 1970s and 1980s while the model warms up quickly after ~year 2000
404 (see Figure 23 of Golaz et al., 2022). The global surface air temperature biases during the past decades in
405 E3SMv1 and v2 have been attributed to the strong aerosol forcing in the model (Golaz et al., 2019; 2022).
406 As the global mean precipitation scales with the surface temperature at ~2% per degree (Allen and Ingram,
407 2002), model biases in surface temperature are reflected in biases in precipitation and hence soil moisture,
408 resulting in similar long-term trends between soil temperature and soil moisture biases in the simulations.

409

410 **3.5 2012 U.S. Midwest Drought**

411 To further evaluate the performance of the WCLDA system, we briefly investigate the impact of land
412 data assimilation on simulating the temporal evolution of the U.S. Midwest drought in 2012. Time series
413 of soil moisture percentiles over the Midwest (36° -50°N, 102° -88°W) demonstrate significant
414 improvements by Assim in reproducing the time evolution of agricultural drought in 2012 compared with
415 CTRL (Figure 10). From the observation based on ERA-Interim data, the agricultural drought starts in
416 August 2011, follows by a brief relief in early spring of 2012, peaks in September 2012, and recovers by
417 January 2013. The drought develops rapidly between May and July 2012 over a wide-spread area
418 including the central and midwestern U.S. This flash drought caused significant agricultural damages and
419 economic losses.

420 The free running CTRL experiment fails to simulate the temporal evolution of the 2012 Midwest
421 drought, with a correlation coefficient between CTRL and observation of only 0.27. The onset and peak
422 of the drought are remarkably well captured by Assim, although the drought recovery occurs two months
423 later than observed. The correlation coefficient of the Assim time series with observation is 0.56, which
424 is statistically significant at the 95% confidence level. Our results highlight the importance of land surface
425 states for drought lifecycle, with the potential to improve future drought predictions through the
426 implementation of the WCLDA system.

427

428 **4 Conclusions**

429 In this study, we developed the 4DVar-based WCLDA system for the E3SMv2 model and
430 evaluated the performance of this WCLDA system. The DRP-4DVar method was employed for
431 implementing 4DVar using the ensemble method rather than the adjoint technique. Special attention is
432 paid to directly assimilating monthly mean land reanalysis data in this system without interpolating to
433 every time step. Within each one-month assimilation window, we assimilate land reanalysis information
434 into the coupled model without breaking the land-atmosphere interaction, which is important for the
435 WCLDA system to be used to understand the potential sources of predictability provided by land.

436 The WCLDA system is conducted from 1980 to 2016, and its performance is evaluated using multiple
437 metrics, including the cost function, AE index, correlation, RMSE and bias. Compared with CTRL, the
438 cost function is reduced by Assim in most months, suggesting that the GLDAS reanalysis data has been
439 effectively incorporated into the model. In terms of both soil moisture and temperature, Assim
440 outperforms CTRL with lower RMSE and higher temporal correlation in many regions, especially in
441 South America, central Africa, Australia, and large parts of Eurasia. For soil moisture bias, Assim further
442 decreases the dry bias during the first twenty years and the wet bias thereafter. It is noteworthy that the
443 subseasonal-to-seasonal time evolution of soil moisture percentiles during the 2012 U.S. Midwest drought
444 can be quite well captured in Assim, underscoring the significant role of land surface states in drought
445 propagation.

446 Our current WCLDA system has some limitations such as the lack of an observation operator to
447 integrate actual observations (e.g., satellite and station data). An observation operator is crucial in

448 providing the linkage between the model variables and actual observations, which differ in spatial and
449 temporal resolutions. Hence future exploration will focus on developing observation operators suitable
450 for assimilating various satellite data, such as the AMSR-E and GRACE data. It is possible that the
451 influence of the WCLDA system on atmospheric processes may be limited in some domains due to
452 uncertainties of the model parameterizations, particularly in representing land-atmosphere interactions
453 (Zhou et al., 2023). For example, in humid regions where the evaporation process is predominantly
454 energy-limited, the assimilation of soil moisture tends to exert limited influence. Instead, the assimilation
455 of soil temperature may yield more substantial improvements. This underscores the importance of the
456 unique characteristics and constraints presented by complicated regional conditions in the application of
457 assimilation processes. To this end, the application of the WCLDA system would motivate future work to
458 better understand the roles of the land surface in climate variability and provide a foundational resource
459 for future predictability studies by the E3SM community.

460

461 *Code and data availability.* The E3SMv2 source codes used in this study can be accessed on Zenodo at
462 <https://zenodo.org/record/8194050>. The GLDAS monthly soil moisture and soil temperature data can be
463 downloaded from the website
464 <https://disc.gsfc.nasa.gov/datasets?keywords=GLDAS%20monthly&page=1>. The GPCP monthly
465 precipitation data are available online (<https://psl.noaa.gov/data/gridded/data.gpcp.html>). The ERA-
466 Interim monthly soil moisture data are available at [https://apps.ecmwf.int/archive-](https://apps.ecmwf.int/archive-catalogue/?levtype=sfc&type=an&class=ei&stream=moda&expver=1)
467 [catalogue/?levtype=sfc&type=an&class=ei&stream=moda&expver=1](https://apps.ecmwf.int/archive-catalogue/?levtype=sfc&type=an&class=ei&stream=moda&expver=1). The model data used in this study
468 can be found on Zenodo at <https://zenodo.org/record/8148737>.

469

470 *Author contributions.* LRL initiated this study. PS and LRL designed the experiments. BW provided
471 advice on the data assimilation technique and KZ and SZ provided assistance with the E3SM model. PS
472 developed the data assimilation code and performed the simulations. PS and LRL analyzed and interpreted
473 the data. PS and LRL wrote the paper. BW, KZ, SMH, and SZ contributed to the revision.

474

475 *Competing interests.* The authors declare no competing interests.

476

477 *Acknowledgements.* This research was supported by the Office of Science, Department of Energy
478 Biological and Environmental Research as part of the Regional and Global Model Analysis program area.
479 Pacific Northwest National Laboratory is operated by Battelle Memorial Institute for the U.S.
480 Department of Energy under contract DE-AC05-76RL01830.

481 **References**

- 482 Allen, M. R., and Ingram, W. J.: Constraints on future changes in climate and the hydrologic cycle, *Nature*,
483 419, 224–232, <https://doi.org/10.1038/nature01092>, 2002.
- 484 Ardilouze, C., Batté, L., Bunzel, F., Decremer, D., Déqué, M., Doblas-Reyes, F. J., Douville, H., Fereday,
485 D., Guemas, V., MacLachlan, C. and Müller, W.: Multi-model assessment of the impact of soil
486 moisture initialization on mid-latitude summer predictability, *Climate Dynamics*, 49, 3959–3974,
487 <https://doi.org/10.1007/s00382-017-3555-7>, 2017.
- 488 Balmaseda, M. A., Alves, O. J., Arribas, A., Awaji, T., Behringer, D. W., Ferry, N., Fujii, Y., Lee, T.,
489 Rienecker, M., Rosati, T. and Stammer, D.: Ocean initialization for seasonal forecasts,
490 *Oceanography*, 22(3), 154–159, <https://doi.org/10.5670/oceanog.2009.73>, 2009.
- 491 Bellucci, A., Gualdi, S., Masina, S., Storto, A., Scoccimarro, E., Cagnazzo, C., Fogli, P., Manzini, E., and
492 Navarra, A.: Decadal climate predictions with a coupled OAGCM initialized with oceanic
493 reanalyses, *Climate Dynamics*, 40, 1483–1497, <https://doi.org/10.1007/s00382-012-1468-z>, 2013.
- 494 Boer, G. J., Smith, D. M., Cassou, C., Doblas-Reyes, F., Danabasoglu, G., Kirtman, B., Kushnir, Y.,
495 Kimoto, M., Meehl, G. A., Msadek, R. and Mueller, W. A.: The decadal climate prediction project
496 (DCPP) contribution to CMIP6, *Geoscientific Model Development*, 9(10), 3751–3777,
497 <https://doi.org/10.5194/gmd-9-3751-2016>, 2016.
- 498 Browne, P. A., De Rosnay, P., Zuo, H., Bennett, A., and Dawson, A.: Weakly coupled ocean-atmosphere
499 data assimilation in the ECMWF NWP system, *Remote Sensing*, 11(3), 234,
500 <https://doi.org/10.3390/rs11030234>, 2019.
- 501 Buehner, M., Du, P., and Bédard, J.: A new approach for estimating the observation impact in ensemble-
502 variational data assimilation, *Monthly Weather Review*, 146(2), 447-465,
503 <https://doi.org/10.1175/MWR-D-17-0252.1>, 2018.
- 504 Carrassi, A., Weber, R. J. T., Guemas, V., Doblas-Reyes, F. J., Asif, M., and Volpi, D.: Full-field and
505 anomaly initialization using a low-order climate model: a comparison and proposals for advanced
506 formulations, *Nonlinear Processes in Geophysics*, 21, 521-537, [https://doi.org/10.5194/npg-21-521-](https://doi.org/10.5194/npg-21-521-2014)
507 2014, 2014.
- 508 Chen, Z., Zeng, Y., Shen, G., Xiao, C., Xu, L., and Chen, N. C.: Spatiotemporal characteristics and

509 estimates of extreme precipitation in the Yangtze River Basin using GLDAS data, *International*
510 *Journal of Climatology*, 41, 1812–1830, <https://doi.org/10.1002/joc.6813>, 2021.

511 Collins, M. and Allen, M. R.: Assessing the relative roles of initial and boundary conditions in interannual
512 to decadal climate predictability, *Journal of Climate*, 15, 3104–3109, [https://doi.org/10.1175/1520-0442\(2002\)015<3104:ATRROI> 2.0.CO;2](https://doi.org/10.1175/1520-0442(2002)015<3104:ATRROI> 2.0.CO;2), 2002.

514 Conil, S., Douville, H., and Tyteca, S.: The relative influence of soil moisture and SST in climate
515 predictability explored within ensembles of AMIP type experiments, *Climate Dynamics*, 28, 125–
516 145, <https://doi.org/10.1007/s00382-006-0172-2>, 2007.

517 Courtier, P., Thépaut, J. M., and Hollingsworth, A.: A strategy for operational implementation of 4D-Var,
518 using an incremental approach, *Quarterly Journal of the Royal Meteorological Society*, 120, 1367–
519 1387, <https://doi.org/10.1002/qj.49712051912>, 1994.

520 Craig, A. P., Vertenstein, M., and Jacob, R.: A new flexible coupler for Earth system modeling developed
521 for CCSM4 and CESM1, *International Journal of High Performance Computing Applications*, 26(1),
522 31–42, <https://doi.org/10.1177/1094342011428141>, 2012.

523 Dee, D. P., Balsameda, M., Balsamo, G., Engelen, R., Simmons, A. J., and Thépaut, J. N.: Toward a
524 consistent reanalysis of the climate system, *Bulletin of the American Meteorological Society*, 95(8),
525 1235-1248, <https://doi.org/10.1175/BAMS-D-13-00043.1>, 2014.

526 Dennis, J. M., Edwards, J., Loy, R., Jacob, R., Mirin, A. A., Craig, A. P., and Vertenstein, M.: An
527 application-level parallel I/O library for Earth system models, *International Journal of High*
528 *Performance Computing Applications*, 26(1), 43–53, <https://doi.org/10.1177/1094342011428143>,
529 2012.

530 Du, H., Doblas-Reyes, F. J., García-Serrano, J., Guemas, V., Soufflet, Y., and Wouters, B.: Sensitivity of
531 decadal predictions to the initial atmospheric and oceanic perturbations, *Climate Dynamics*, 39(7),
532 2013–2023, <https://doi.org/10.1007/s00382-011-1285-9>, 2012.

533 Edwards, A. C., Scalenghe, R., and Freppaz, M.: Changes in the seasonal snow cover of alpine regions
534 and its effect on soil processes: a review, *Quaternary International*, 162, 172–181,
535 <https://doi.org/10.1016/j.quaint.2006.10.027>, 2007.

536 Eyring, V., Bony, S., Meehl, G. A., Senior, C. A., Stevens, B., Stouffer, R. J., and Taylor, K. E.: Overview

537 of the Coupled Model Intercomparison Project Phase 6 (CMIP6) experimental design and
538 organization, *Geoscientific Model Development*, 9, 1937–1958, [https://doi.org/10.5194/gmd-9-](https://doi.org/10.5194/gmd-9-1937-2016)
539 1937-2016, 2016.

540 Fowler, A. M., and Lawless, A. S.: An idealized study of coupled atmosphere–ocean 4D-Var in the
541 presence of model error, *Monthly Weather Review*, 144(10), 4007–4030,
542 <https://doi.org/10.1175/MWR-D-15-0420.1>, 2016.

543 Giroto, M., De Lannoy, G. J., Reichle, R. H., and Rodell, M.: Assimilation of gridded terrestrial water
544 storage observations from GRACE into a land surface model, *Water Resources Research*, 52(5),
545 4164–4183, <https://doi.org/10.1002/2015WR018417>, 2016.

546 Golaz, J. C., Caldwell, P. M., Van Roekel, L. P., Petersen, M. R., Tang, Q., Wolfe, J. D., Abeshu, G.,
547 Anantharaj, V., Asay-Davis, X. S., Bader, D. C., Baldwin, S. A., Bisht, G., Bogenschutz, P. A.,
548 Branstetter, M., Brunke, M. A., Brus, S. R., Burrows, S. M., Cameron-Smith, P. J., Donahue, A. S.,
549 Deakin, M., Easter, R. C., Evans, K. J., Feng, Y., Flanner, M., Foucar, J. G., Fyke, J. G., Griffin, B.
550 M., Hannay, C., Harrop, B. E., Hoffman, M. J., Hunke, E. C., Jacob, R. L., Jacobsen, D. W., Jeffery,
551 N., Jones, P. W., Keen, N. D., Klein, S. A., Larson, V. E., Leung, L. R., Li, H. Y., Lin, W., Lipscomb,
552 W. H., Ma, P. L., Mahajan, S., Maltrud, M. E., Mametjanov, A., McClean, J. L., McCoy, R. B.,
553 Neale, R. B., Price, S. F., Qian, Y., Rasch, P. J., Reeves Eyre, J. E. J., Riley, W. J., Ringler, T. D.,
554 Roberts, A. F., Roesler, E. L., Salinger, A. G., Shaheen, Z., Shi, X., Singh, B., Tang, J., Taylor, M.
555 A., Thornton, P. E., Turner, A. K., Veneziani, M., Wan, H., Wang, H., Wang, S., Williams, D. N.,
556 Wolfram, P. J., Worley, P. H., Xie, S., Yang, Y., Yoon, J.-H., Zelinka, M. D., Zender, C. S., Zeng, X.,
557 Zhang, C., Zhang, K., Zhang, Y., Zheng, X., Zhou, T., and Zhu, Q.: The DOE E3SM Coupled Model
558 Version 1: Overview and Evaluation at Standard Resolution, *Journal of Advances in Modeling Earth
559 Systems*, 11, 2089–2129, <https://doi.org/https://doi.org/10.1029/2018MS001603>, 2019.

560 Golaz, J. C., Van Roekel, L. P., Zheng, X., Roberts, A. F., Wolfe, J. D., Lin, W. Y., Bradley, A. M., Tang,
561 Q., Maltrud, M. E., Forsyth, R. M., Zhang, C. Z., Zhou, T., Zhang, K., Zender, C. S., Wu, M. X.,
562 Wang, H. L., Turner, A. K., Singh, B., Richter, J. H., Qin, Y., Petersen, M. R., Mametjanov, A., Ma,
563 P., Larson, V. E., Krishna, J., Keen, N. D., Jeffery, N., Hunke, E. C., Hannah, W. M., Guba, O.,
564 Griffin, B. M., Feng, Y., Engwirda, D., Vittorio, A. V., Cheng, D., Conlon, L. M., Chen, C., Brunke,

565 M. A., Bisht, G., Benedict, J. J., Asay-Davis, X. S., Zhang, Y. Y., Zhang, M., Zeng, X. B., Xie, S.
566 C., Wolfram, P. J., Vo, T., Veneziani, M., Tesfa, T. K., Sreepathi, S., Salinger, A. G., Jack Reeves
567 Eyre, J. E., Prather, M. J., Mahajan, S., Li, Q., Jones, P. W., Jacob, R. L., Huebler, G. W., Huang, X.
568 L., Hillman, B. R., Harrop, B. E., Foucar, J. G., Fang, Y. L., Comeau, D. S., Caldwell, P. M.,
569 Bartoletti, T., Balaguru, K., Taylor, M. A., McCoy, R. B., Leung, L. R., and Bader, D. C.: The DOE
570 E3SM Model version 2: Overview of the physical model and initial model evaluation, *Journal of*
571 *Advances in Modeling Earth Systems*, 14, e2022MS003156, <https://doi.org/10.1029/2022MS003156>, 2022.

573 Guo, Z., Dirmeyer, P. A., Delsole, T., and Koster, R. D.: Rebound in atmospheric predictability and the
574 role of the land surface, *Journal of Climate*, 25(13), 4744–4749, [https://doi.org/10.1175/JCLI-D-11-](https://doi.org/10.1175/JCLI-D-11-00651.1)
575 00651.1, 2012.

576 He, Y., Wang, B., Liu, M., Liu, L., Yu, Y., Liu, J., Li, R., Zhang, C., Xu, S., Huang, W., Liu, Q., Wang,
577 Y., and Li, F.: Reduction of initial shock in decadal predictions using a new initialization strategy,
578 *Geophysical Research Letters*, 44(16), 8538–8547, <https://doi.org/10.1002/2017GL074028>, 2017.

579 He, Y., Wang, B., Liu, L., Huang, W., Xu, S., Liu, J., Wang, Y., Li, L., Huang, X., Peng, Y., Lin, Y., and
580 Yu, Y.: A DRP-4DVar-based coupled data assimilation system with a simplified off-line localization
581 technique for decadal predictions, *Journal of Advances in Modeling Earth Systems*, 12(4),
582 e2019MS001768, <https://doi.org/10.1029/2019MS001768>, 2020a.

583 He, Y., Wang, B., Huang, W., Xu, S., Wang, Y., Liu, L., Li, L., Liu, J., Yu, Y., Lin, Y., Huang, X., and
584 Peng, Y.: A new DRP-4DVar-based coupled data assimilation system for decadal predictions using
585 a fast online localization technique, *Climate Dynamics*, 54, 3541–3559,
586 <https://doi.org/10.1007/s00382-020-05190-w>, 2020b.

587 Hoke, J. E. and Anthes, R. A.: The initialization of numerical models by a dynamic-initialization
588 technique, *Monthly Weather Review*, 104(12), 1551–1556, [https://doi.org/10.1175/1520-](https://doi.org/10.1175/1520-0493(1976)104<1551:TIONMB>2.0.CO;2)
589 0493(1976)104<1551:TIONMB>2.0.CO;2, 1976.

590 Houborg, R., Rodell, M., Li, B., Reichle, R., and Zaitchik, B. F.: Drought indicators based on model-
591 assimilated Gravity Recovery and Climate Experiment (GRACE) terrestrial water storage
592 observations, *Water Resources Research*, 48, W07525, <https://doi.org/10.1029/2011WR011291>,

593 2012.

594 Hu, S., Zhou, T., and Wu, B.: Improved ENSO prediction skill resulting from reduced climate drift in
595 IAP-DecPreS: A comparison of full-field and anomaly initializations, *Journal of Advances in*
596 *Modeling Earth Systems*, 12, e2019MS001759, <https://doi.org/10.1029/2019MS001759>, 2020.

597 Ireson, A. M., Van Der Kamp, G., Ferguson, G., Nachshon, U., and Wheeler, H. S.: Hydrogeological
598 processes in seasonally frozen northern latitudes: understanding, gaps and challenges,
599 *Hydrogeology Journal*, <https://doi.org/10.1007/s10040-012-0916-5>, 2013.

600 Kwon, Y., Yang, Z. L., Zhao, L., Hoar, T. J., Toure, A. M., and Rodell, M.: Estimating snow water storage
601 in North America using CLM4, DART, and snow radiance data assimilation, *Journal of*
602 *Hydrometeorology*, 17(11), 2853–2874, <https://doi.org/10.1175/JHM-D-16-0028.1>, 2016.

603 Laloyaux, P., Balmaseda, M., Dee, D., Mogensen, K., and Janssen, P.: A coupled data assimilation system
604 for climate reanalysis, *Quarterly Journal of the Royal Meteorological Society*, 142(694), 65-78,
605 <https://doi.org/10.1002/qj.2629>, 2016.

606 Lea, D. J., Mirouze, I., Martin, M. J., King, R. R., Hines, A., Walters, D., and Thurlow, M.: Assessing a
607 new coupled data assimilation system based on the Met Office coupled atmosphere–land–ocean–
608 sea ice model, *Monthly Weather Review*, 143(11), 4678-4694, [https://doi.org/10.1175/MWR-D-15-](https://doi.org/10.1175/MWR-D-15-0174.1)
609 0174.1, 2015.

610 Lei, L. L. and Hacker, J. P.: Nudging, ensemble, and nudging ensembles for data assimilation in the
611 presence of model error, *Monthly Weather Review*, 143(7), 2600–2610,
612 <https://doi.org/10.1175/MWR-D-14-00295.1>, 2015.

613 Leung, L. R., Bader, D. C., Taylor, M. A., and McCoy, R. B.: An introduction to the E3SM special
614 collection: Goals, science drivers, development, and analysis, *Journal of Advances in Modeling*
615 *Earth Systems*, 12(11), e2019MS001821, <https://doi.org/10.1029/2019MS001821>, 2020.

616 Li, F., Wang, B., He, Y., Huang, W., Xu, S., Liu, L., Liu, J. and Li, L.: Important role of North Atlantic
617 air–sea coupling in the interannual predictability of summer precipitation over the eastern Tibetan
618 Plateau, *Climate Dynamics*, 56, 1433–1448, <https://doi.org/10.1007/s00382-020-05542-6>, 2021.

619 Li, H. Y., Wigmosta, M. S., Wu, H., Huang, M., Ke, Y., Coleman, A. M., and Leung, L. R.: A physically
620 based runoff routing model for land surface and Earth system models, *Journal of Hydrometeorology*,

621 14, 808–828, <https://doi.org/10.1175/JHM-D-12-015.1>, 2013.

622 Lin, L. F., Ebtehaj, A. M., Wang, J., and Bras, R. L.: Soil moisture background error covariance and data
623 assimilation in a coupled land-atmosphere model, *Water Resources Research*, 53(2), 1309–1335,
624 <https://doi.org/10.1002/2015WR017548>, 2017.

625 Lin, P., Yang, Z. L., Wei, J., Dickinson, R. E., Zhang, Y., and Zhao, L.: Assimilating multi-satellite snow
626 data in ungauged Eurasia improves the simulation accuracy of Asian monsoon seasonal anomalies,
627 *Environmental Research Letters*, 15(6), 064033, <https://doi.org/10.1088/1748-9326/ab80ef>, 2020.

628 Liu, D., and Mishra, A. K.: Performance of AMSR_E soil moisture data assimilation in CLM4. 5 model
629 for monitoring hydrologic fluxes at global scale, *Journal of Hydrometeorology*, 547, 67–79,
630 <https://doi.org/10.1016/j.jhydrol.2017.01.036>, 2017.

631 Liu, J. J., Wang, B., and Xiao, Q. N.: An evaluation study of the DRP-4-DVar approach with the Lorenz-
632 96 model, *Tellus A: Dynamic Meteorology and Oceanography*, 63, 256–262,
633 <https://doi.org/10.1111/j.1600-0870.2010.00487.x>, 2011.

634 Lorenc, A. C., Bowler, N. E., Clayton, A. M., Pring, S. R., and Fairbairn, D.: Comparison of hybrid-
635 4D-EnVar and hybrid-4D-Var data assimilation methods for global NWP, *Monthly Weather Review*,
636 143, 212–229, <https://doi.org/10.1175/MWR-D-14-00195.1>, 2015.

637 Mochizuki, T., Masuda, S., Ishikawa, Y., and Awaji, T.: Multiyear climate prediction with initialization
638 based on 4D-Var data assimilation, *Geophysical Research Letters*, 43(8), 3903–3910,
639 <https://doi.org/10.1002/2016GL067895>, 2016.

640 Oleson, K. W., Lawrence, D. M., Bonan, G. B., Drewniak, B., Huang, M., Koven, C. D., Levis, S., Li,
641 F., Riley, W. J., Subin, Z. M., Swenson, S. C., Thornton, P. E., Bozbiyik, A., Fisher, R., Heald, C.
642 L., Kluzek, E., Lamarque, J. F., Lawrence, P. J., Leung, L. R., Lipscomb, W., Muszala, S., Ricciuto,
643 D. M., Sacks, W., Sun, Y., Tang, J., and Yang, Z. L.: Technical description of version 4.5 of the
644 Community Land Model (CLM) (Tech. Rep. NCAR/TN-503+STR). Boulder, Colorado, USA:
645 National Center for Atmospheric Research, <http://dx.doi.org/10.5065/D6RR1W7M>, 2013.

646 Penny, S. G., and Hamill, T. M.: Coupled data assimilation for integrated earth system analysis and
647 prediction, *Bulletin of the American Meteorological Society*, 98(7), ES169–ES172,
648 <https://doi.org/10.1175/BAMS-D-17-0036.1>, 2017.

649 Penny, S. G., Bach, E., Bhargava, K., Chang, C. C., Da, C., Sun, L., and Yoshida, T.: Strongly coupled
650 data assimilation in multiscale media: Experiments using a quasi-geostrophic coupled model,
651 Journal of Advances in Modeling Earth Systems, 11(6), 1803-1829,
652 <https://doi.org/10.1029/2019MS001652>, 2019.

653 Petersen, M., Asay-Davis, X. S., Jacobsen, D., Maltrud, M., Ringler, T., Van Roekel, L., and Wolfram,
654 P.: MPAS ocean user's guide V6, Zenodo, <https://doi.org/10.5281/zenodo.1246893>, 2018.

655 Polkova, I., Köhl, A., and Stammer, D.: Climate-mode initialization for decadal climate predictions,
656 Climate Dynamics, 53, 7097–7111, <https://doi.org/10.1007/s00382-019-04975-y>, 2019.

657 Reckinger, S. M., Petersen, M. R., and Reckinger, S. J.: A study of overflow simulations using MPAS-
658 Ocean: Vertical grids, resolution, and viscosity, Ocean Modeling, 96, 291–313,
659 <https://doi.org/10.1016/j.ocemod.2015.09.006>, 2015.

660 Rodell, M., Houser, P. R., Jambor, U., Gottschalck, J., Mitchell, K., Meng, C. J., Arsenault, K., Cosgrove,
661 B., Radakovich, J., Bosilovich, M. and Entin, J. K., Walker, J. P., Lohmann, D., and Toll, D.: The
662 global land data assimilation system, Bulletin of the American Meteorological society, 85(3), 381–
663 394, <https://doi.org/10.1175/BAMS-85-3-381>, 2004.

664 Sakaguchi, K., Zeng, X., and Brunke, M. A.: The hindcast skill of the CMIP ensembles for the surface
665 air temperature trend, Journal of Geophysical Research: Atmospheres, 117, D1611,
666 <https://doi.org/10.1029/2012JD017765>, 2012.

667 Shi, P. F., Wang, B., He, Y., Lu, H., Yang, K., Xu, S. M., Huang, W. Y., Liu, L., Liu, J. J., Li, L. J., and
668 Wang, Y.: Contributions of weakly coupled data assimilation-based land initialization to interannual
669 predictability of summer climate over Europe, Journal of Climate, 35, 517–535,
670 <https://doi.org/10.1175/JCLI-D-20-0506.1>, 2022.

671 Simmons, A. J. and Hollingsworth, A.: Some aspects of the improvement in skill of numerical weather
672 prediction, Quarterly Journal of the Royal Meteorological Society, 128(580), 647–677,
673 <https://doi.org/10.1256/003590002321042135>, 2002.

674 Sluka, T. C., Penny, S. G., Kalnay, E., and Miyoshi, T.: Assimilating atmospheric observations into the
675 ocean using strongly coupled ensemble data assimilation, Geophysical Research Letters, 43(2), 752-
676 759, <https://doi.org/10.1002/2015GL067238>, 2016.

677 Smith, P. J., Fowler, A. M., and Lawless, A. S.: Exploring strategies for coupled 4DVar data assimilation
678 using an idealised atmosphere–ocean model, *Tellus A*, 67(1):27025,
679 <https://doi.org/10.3402/tellusa.v67.27025>, 2015.

680 Smith, D. M., Eade, R., and Pohlmann, H.: A comparison of full-field and anomaly initialization for
681 seasonal to decadal climate prediction, *Climate Dynamics*, 41, 3325–3338,
682 <https://doi.org/10.1007/s00382-013-1683-2>, 2013.

683 Sugiura, N., Awaji, T., Masuda, S., Mochizuki, T., Toyoda, T., Miyama, T., Igarashi, H. and Ishikawa, Y.:
684 Development of a four-dimensional variational coupled data assimilation system for enhanced
685 analysis and prediction of seasonal to interannual climate variations, *Journal of Geophysical*
686 *Research: Oceans*, 113, C10017, <https://doi.org/10.1029/2008JC004741>, 2008.

687 Taylor, K. E., Stouffer, R. J., and Meehl, G. A.: An overview of CMIP5 and the experiment design,
688 *Bulletin of the American Meteorological Society*, 93(4), 485–498, <https://doi.org/10.1175/BAMS->
689 [D-11-00094.1](https://doi.org/10.1175/BAMS-D-11-00094.1), 2012.

690 Taylor, M. A., Guba, O., Steyer, A., Ullrich, P. A., Hall, D. M., and Eldrid, C.: An energy consistent
691 discretization of the nonhydrostatic equations in primitive variables, *Journal of Advances in*
692 *Modeling Earth Systems*, 12, e2019MS001783, <https://doi.org/10.1029/2019MS001783>, 2020.

693 Volpi, D., Guemas, V., and Doblas-Reyes, F. J.: Comparison of full field and anomaly initialisation for
694 decadal climate prediction: towards an optimal consistency between the ocean and sea-ice anomaly
695 initialisation state, *Climate Dynamics*, 49, 1181–1195, <https://doi.org/10.1007/s00382-016-3373-3>,
696 2017.

697 Wang, B., Liu, J., Wang, S., Cheng, W., Liu, J., Liu, C., Xiao, Q., and Kuo, Y. H.: An economical approach
698 to four-dimensional variational data assimilation, *Advances in Atmospheric Sciences*, 27, 715–727,
699 <https://doi.org/10.1007/s00376-009-9122-3>, 2010.

700 Wang, B., Liu, J., Liu, L., Xu, S., and Huang, W.: An approach to localization for ensemble-based data
701 assimilation, *PloS one*, 13(1), e0191088, <https://doi.org/10.1371/journal.pone.0191088>, 2018.

702 Wang, G., Dolman, A. J., Blender, R., and Fraedrich, K.: Fluctuation regimes of soil moisture in ERA-
703 40 reanalysis data, *Theoretical and Applied Climatology*, 99, 1–8, <https://doi.org/10.1007/s00704->
704 [009-0111-3](https://doi.org/10.1007/s00704-009-0111-3), 2010.

705 Yao, Y., Luo, Y., Huang, J., and Ma, J.: Improving the downscaled springtime temperature in Central
706 Asia through assimilating meteorological and snow cover observations, *Atmospheric Research*, 258,
707 105619, <https://doi.org/10.1016/j.atmosres.2021.105619>, 2021.

708 Yin, J., Zhan, X., Zheng, Y., Liu, J., Hain, C. R., and Fang, L.: Impact of quality control of satellite soil
709 moisture data on their assimilation into land surface model, *Geophysical Research Letters*, 41(20),
710 7159–7166, <https://doi.org/10.1002/2014GL060659>, 2014.

711 Yoshida, T., and Kalnay, E.: Correlation-cutoff method for covariance localization in strongly coupled
712 data assimilation, *Monthly Weather Review*, 146(9), 2881-2889, [https://doi.org/10.1175/MWR-D-](https://doi.org/10.1175/MWR-D-17-0365.1)
713 17-0365.1, 2018.

714 Zeng, X., and Decker, M.: Improving the numerical solution of soil moisture–based Richards equation
715 for land models with a deep or shallow water table, *Journal of Hydrometeorology*, 10, 308–319,
716 <https://doi.org/10.1175/2008JHM1011.1>, 2009.

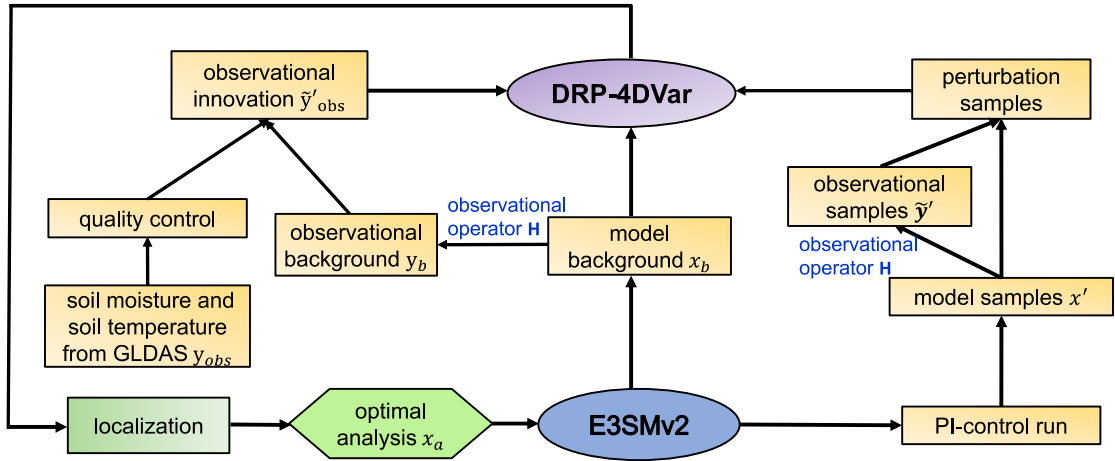
717 Zhang, H., Zhang, L. L., Li, J., An, R. D., Deng, Y.: Climate and Hydrological Change Characteristics
718 and Applicability of GLDAS Data in the Yarlung Zangbo River Basin, China, *Water*, 10, 254,
719 <https://doi.org/10.3390/w10030254>, 2018.

720 Zhang, S., Harrison, M. J., Wittenberg, A. T., Rosati, A., Anderson, J. L., and Balaji, V.: Initialization of
721 an ENSO forecast system using a parallelized ensemble filter, *Monthly Weather Review*, 133(11),
722 3176-3201, <https://doi.org/10.1175/MWR3024.1>, 2005.

723 Zhang, S., Harrison, M. J., Rosati, A., and Wittenberg, A.: System design and evaluation of coupled
724 ensemble data assimilation for global oceanic climate studies, *Monthly Weather Review*, 135(10),
725 3541-3564, <https://doi.org/10.1175/MWR3466.1>, 2007.

726 Zhang, S., Liu, Z., Zhang, X., Wu, X., Han, G., Zhao, Y., Yu, X., Liu, C., Liu, Y., Wu, S., Lu, F., Li, M.,
727 Deng, X.: Coupled data assimilation and parameter estimation in coupled ocean–atmosphere models:
728 a review, *Climate Dynamics*, 54, 5127-5144, <https://doi.org/10.1007/s00382-020-05275-6>, 2020.

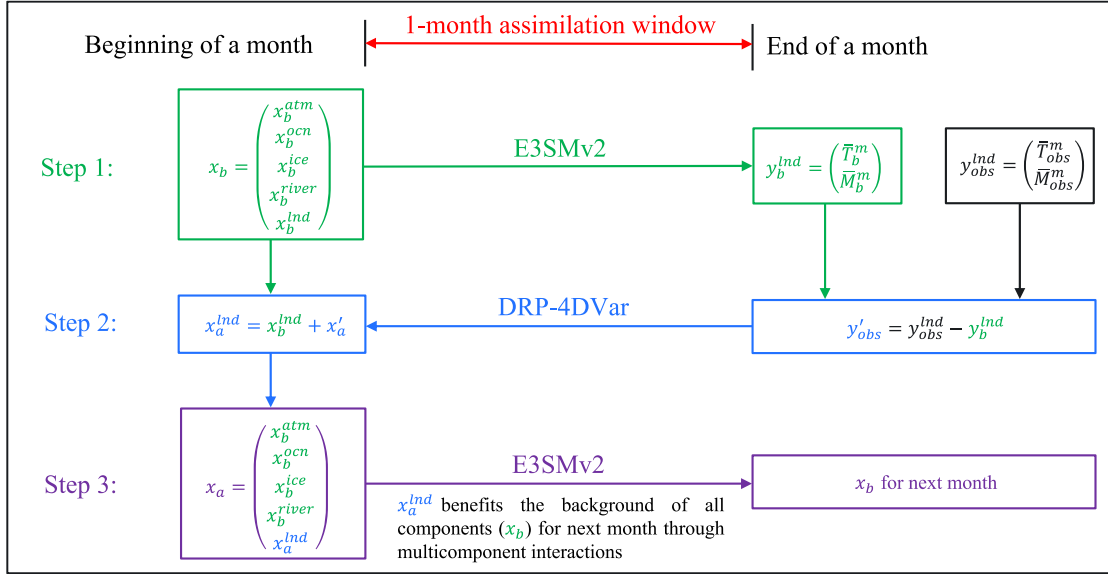
729 Zhou, J., Yang, K., Crow, W.T., Dong, J., Zhao, L., Feng, H., Zou, M., Lu, H., Tang, R. and Jiang, Y.:
730 Potential of remote sensing surface temperature-and evapotranspiration-based land-atmosphere
731 coupling metrics for land surface model calibration, *Remote Sensing of Environment*, 291, 113557,
732 <https://doi.org/10.1016/j.rse.2023.113557>, 2023.



733

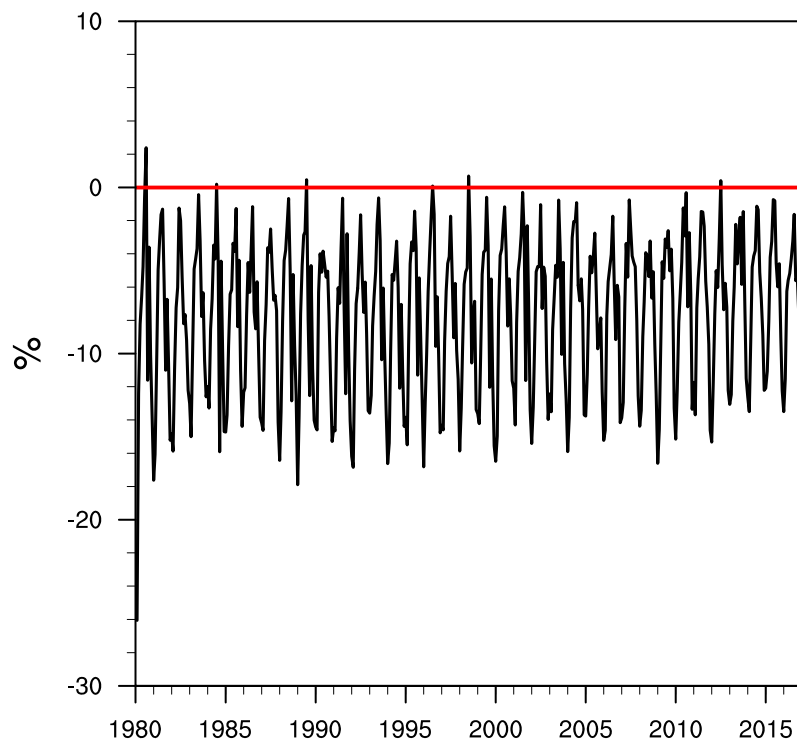
734 **Figure 1.** Flowchart of the 4DVar-based WCLDA system in E3SMv2 based on the DRP-4DVar

735 method.



736

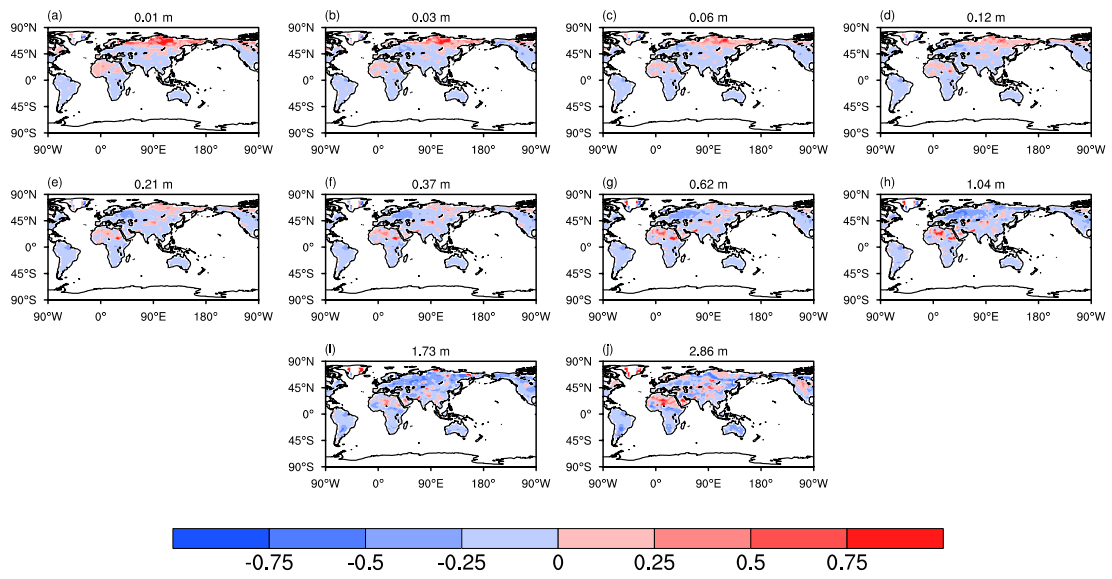
737 **Figure 2.** Schematic flowchart of the 4DEnVar-based WCLDA system. The beginning of a month is at
 738 0000 UTC on the first day of the month, and the end of the month is at 0000 UTC on the first day of the
 739 next month. x_b denotes the background vector including the backgrounds of all E3SMv2 components
 740 (atmosphere (x_b^{atm}), ocean (x_b^{ocn}), sea ice (x_b^{ice}), river transport (x_b^{river}) and land surface (x_b^{lnd})). x_a
 741 consists of the assimilation analysis of land surface (x_a^{lnd}) and the backgrounds of other components.
 742 y_b^{lnd} represents the simulated monthly mean soil temperature (\bar{T}_b^m) and moisture (\bar{M}_b^m) by E3SMv2 using
 743 x_b as the initial condition. y_{obs}^{lnd} denotes the monthly mean GLDAS data of soil temperature (\bar{T}_{obs}^m) and
 744 moisture (\bar{M}_{obs}^m). y'_{obs} denotes the observational innovation, which is the difference between the GLDAS
 745 data (y_{obs}^{lnd}) and the observational background (y_b^{lnd}).



746

747 **Figure 3.** Time series of the reduction rate of the cost function from 1980 to 2016 in the 4DEnVar-based

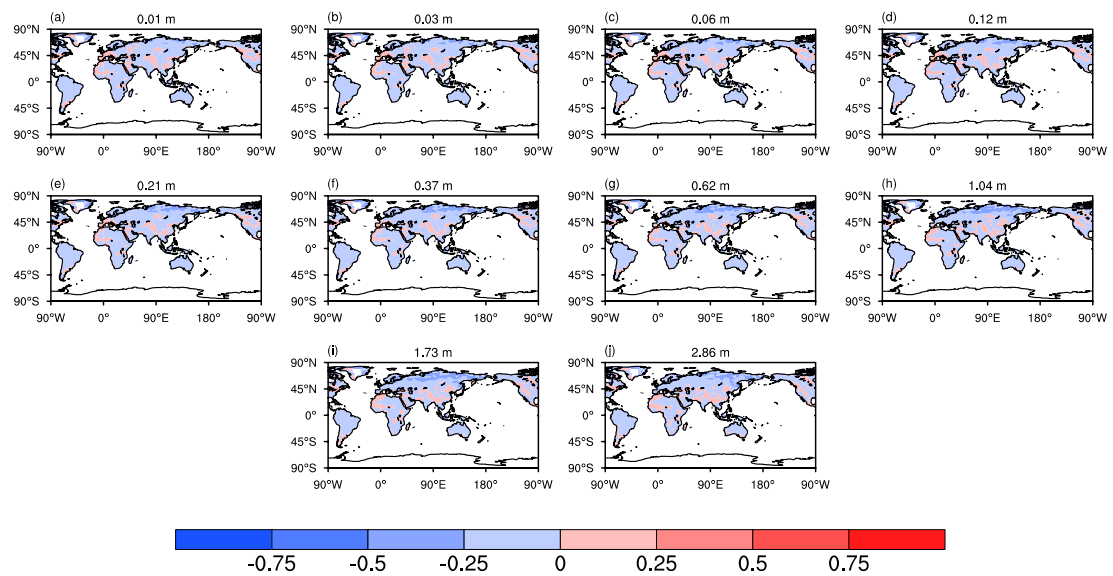
748 WCLDA system.



749

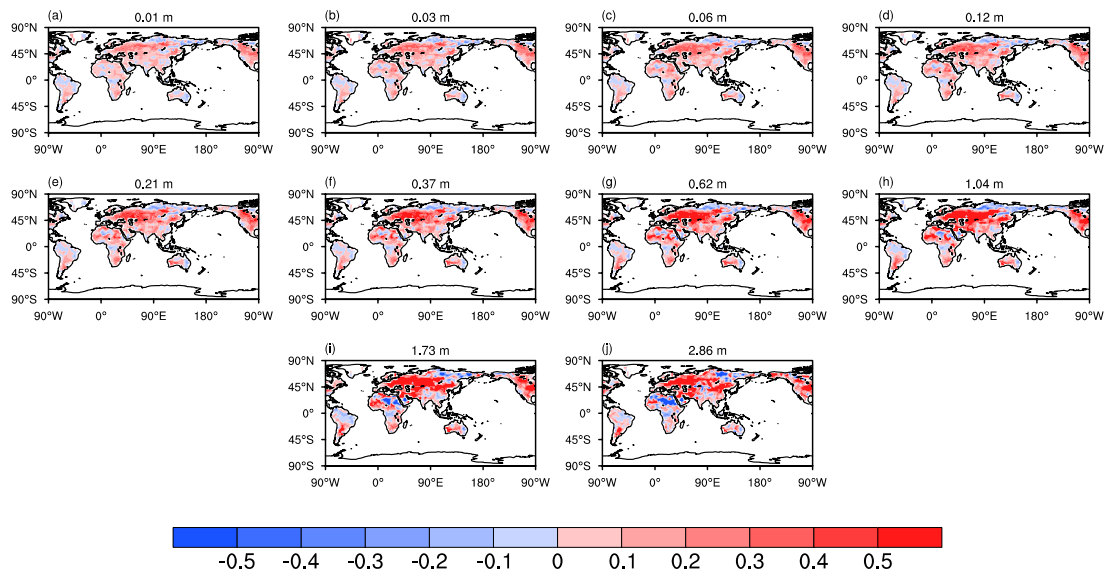
750 **Figure 4.** Spatial distribution of the AE index for soil moisture from the surface to deep layers during

751 the 1980-2016 period. The number at the top center denotes the depth of each soil layer.



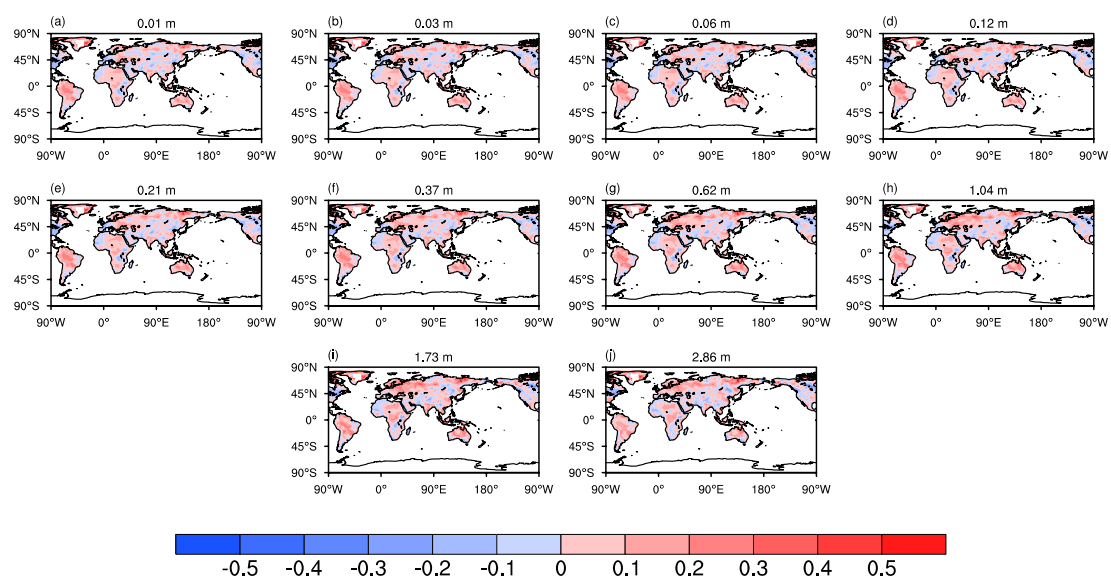
752

753 **Figure 5.** Same as in Figure 4, but for soil temperature.



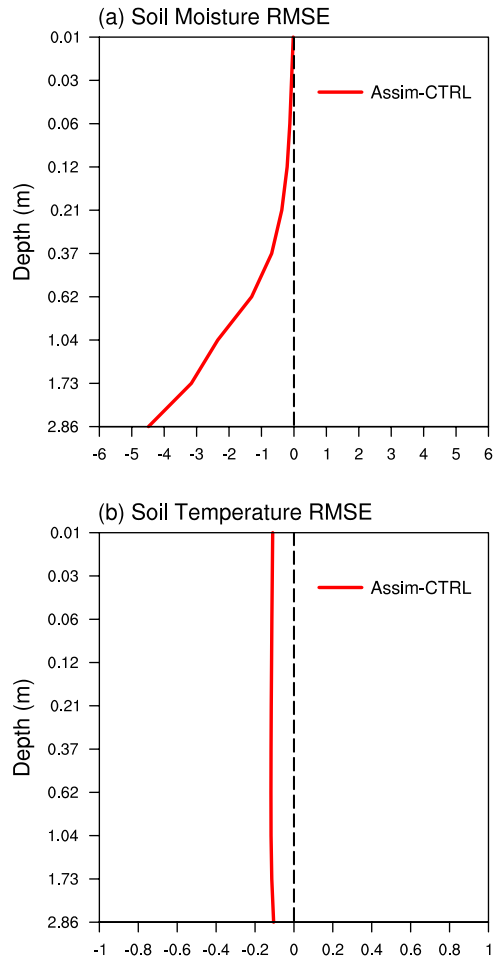
754

755 **Figure 6.** Differences between correlations of soil moisture in Assim and CTRL with the GLDAS data
 756 from the surface to deep layers for the period of 1980-2016. The number at the top center denotes the
 757 depth of each soil layer.



758

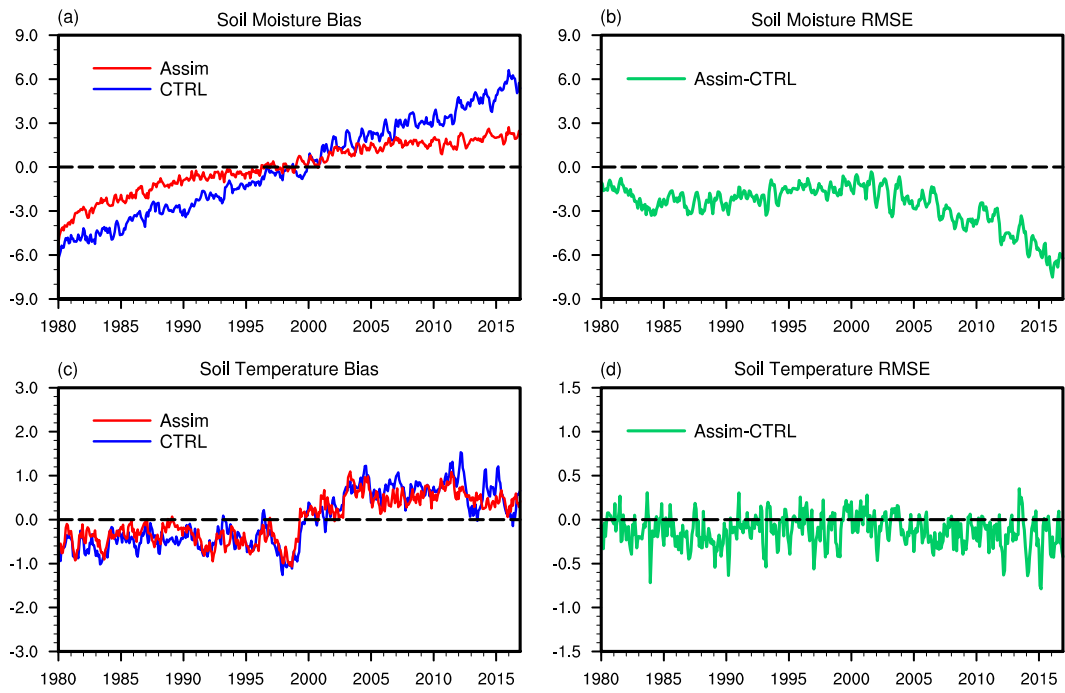
759 **Figure 7.** Same as in Figure 6, but for soil temperature.



760

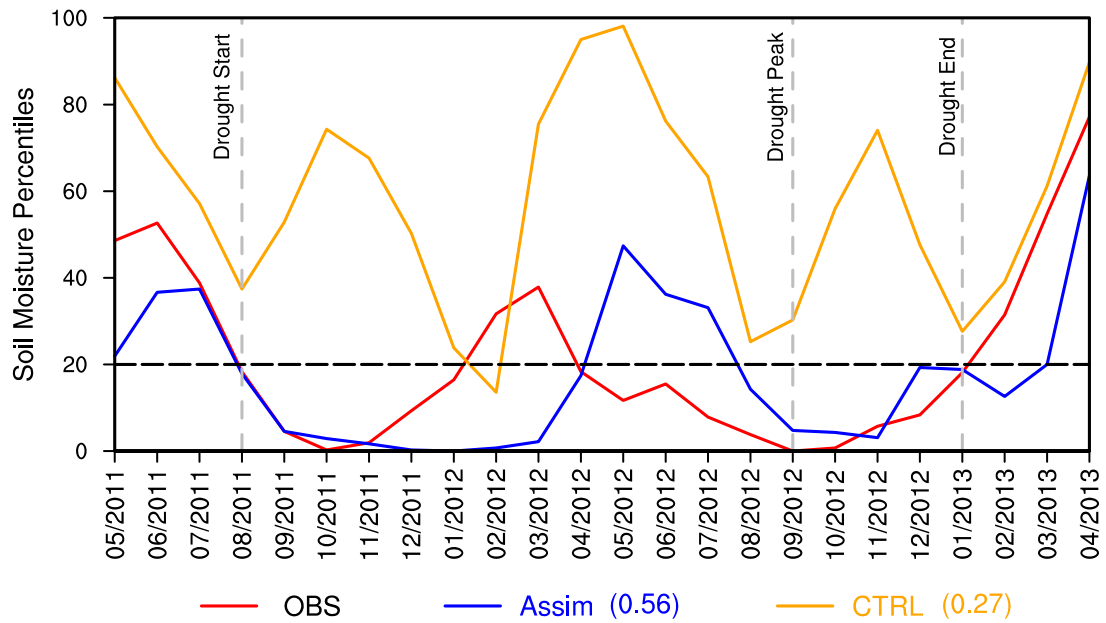
761 **Figure 8.** Vertical distributions of RMSE differences (Assim minus CTRL) for (a) soil moisture and (b)

762 soil temperature averaged over the global land during the 1980-2016 period.



763

764 **Figure 9.** Time series of the vertically averaged global mean soil moisture and temperature bias (left) for
 765 Assim (red line) and CTRL (blue line), and RMSE differences (right, green line) between Assim and
 766 CTRL from 1980 to 2016.



767

768 **Figure 10.** Time series of soil moisture percentiles between May 2011 and April 2013 during the 2012

769 U.S. Midwest drought. Red line: observation, blue line: Assim, orange line: CTRL. The correlation

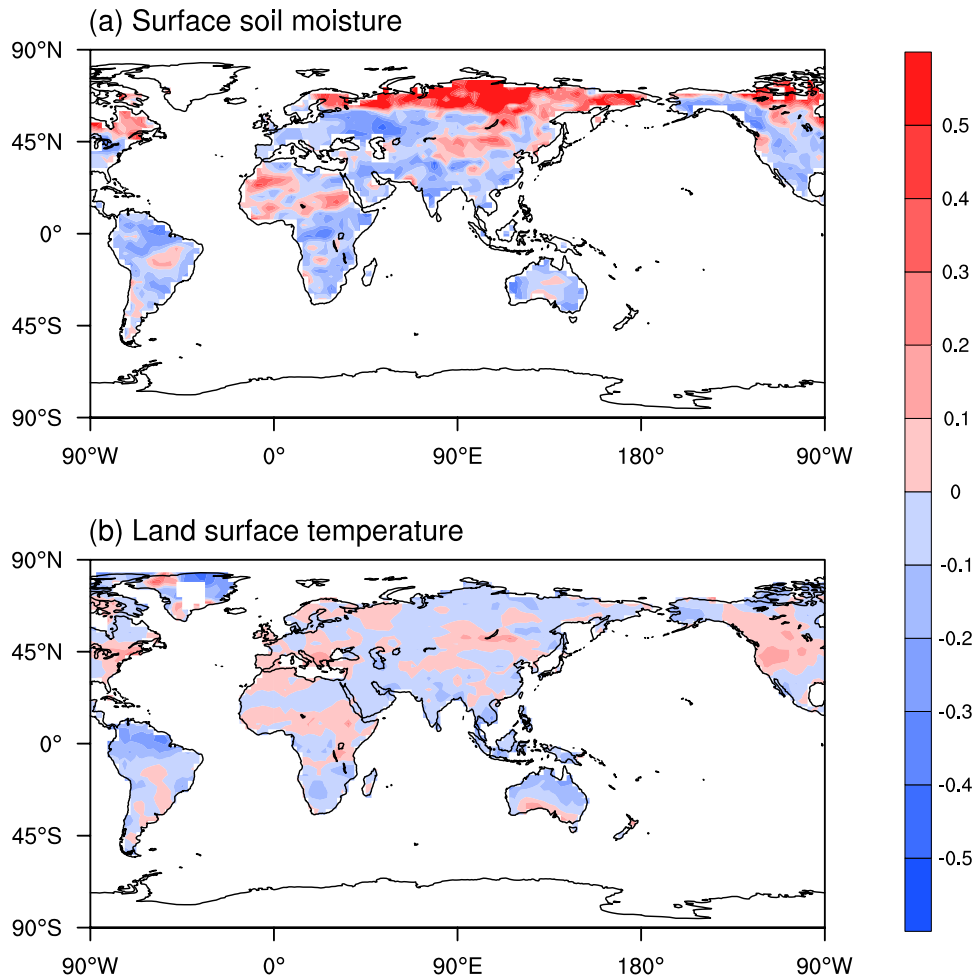
770 coefficients of Assim and CTRL with observations are also shown. The three vertical dashed lines mark

771 the timing of drought start, drought peak and drought end, respectively. The start of the agricultural

772 drought is defined as the month when soil moisture falls below the 20th percentile. The soil moisture

773 percentiles are averaged over the U.S. Midwest (36°-50°N, 102°-88°W). The observed soil moisture is

774 derived from ERA-Interim monthly soil moisture data.



776

777 **Figure A1.** Spatial distribution of the AE index for (a) surface soil moisture and (b) land surface

778 temperature during the 2003-2014 period. The observations are derived from monthly MODIS satellite

779 data.